Super-Resolution Ultrasound Localisation Microscopy of Microvascular Structure and Flow for Distinguishing Metastatic Lymph Nodes – an Initial in Human Study

1. Introduction

The lymph node (LN) is a key route for cancer metastasis and LN status is one of the most important indicators of prognosis in patients who are diagnosed with cancer. Currently, various modalities are used to characterise LN, including ultrasound (US), magnetic resonance imaging (MRI), computed tomography (CT) and positron emission tomography (PET). Liao [1] has reported that, for differentiating between benign and malignant LNs, the sensitivities of existing modalities US, MRI, CT and PET were low (<=66%). Invasive procedures such as LN dissection and excisional sentinel LN biopsy are routinely used for the diagnosis and management of cancer patients, despite the fact that many cancer patients do not have LN metastases at the time of diagnosis [2][3]. Besides cost of such invasive procedures, they can also cause complications like infection, lymphoedema and sensory loss [2][4]. Hence, there is a pressing clinical need of an advanced non-invasive imaging modality to accurately characterise LN diseases.

Angiogenesis plays a fundamental role in the development of the chaotic and irregular vessel structure [5] and can contribute to the early detection, diagnosis and prognosis of cancer[6] . From a physiological point of view, vessels whose function is of great significance for tissue integrity often lie at the perfusion level. Hence, non-invasive imaging of microvasculature can potentially address the aforementioned clinical need in LN characterisation.

Contrast-enhanced ultrasound (CEUS) has emerged to be a valuable tool for imaging flow and tissue perfusion in vivo [7]. CEUS has been used for imaging human lymph system e.g. for identifying sentinel LNs [8], and for distinguishing benign and malignant LNs [9]. However,

due to various confounding factors in CEUS imaging [10], objective and quantitative clinical assessment of the images is challenging and inconsistent results have been reported in different studies [11]. Furthermore, existing clinical CEUS has limited spatial resolution, making characterisation of LNs (some <1cm) difficult.

Optical super-resolution has revolutionised the field of fluorescence microscopy [12]. Its acoustic counterpart, super-resolution ultrasound (SRUS), localizes and tracks individual microbubbles, enabling the quantification of micro-vascular structure and flow far beyond the wave diffraction resolution limit [13]. Notably, among many studies are the first demonstration of super-localisation in vivo [14], and the first demonstration of super-resolution by separating two closely positioned structures, as well as super-resolved velocity mapping [15-16]. A number of following studies have demonstrated the feasibility of SRUS in vivo in animal models [17-22] including tumour models [17][21][22], in healthy volunteers [23] and in breast cancer patients [21]. Recently phase change nanodroplets have also been used for real-time SRUS [24].

Volumetric SRUS images of LN vascular structure and flow dynamics have been demonstrated in a scanning 2D imaging approach on a rabbit model [19], offering a spatial resolution of < 30 microns. Non-invasive SRUS imaging with such resolution in deep tissue has great potential to improve the management of e.g. cancer patients. However, the use of SRUS for human LN imaging to distinguish different pathology have not been reported.

In this study we hypothesised that the application of SRUS imaging enables quantitative markers to distinguish metastatic LNs from benign (reactive) ones in patients with lymphadenopathy.

2. Materials and methods

2.1 Clinical data acquisition

The CEUS data acquisitions were performed on patients (Table1) with suspected lymphadenopathy between March 2019 and September 2019 at the XXX Hospital XXX. Ethics was approved by the University Institutional Ethics Board. Informed consents were signed by the participants before the ultrasound examination.

Ultrasound examinations were performed using a clinical scanner (Mindray Resona 7S) which provides live dual images of B-mode and CEUS. A L11-3U transducer was used with a transmit central frequency of 5.6 MHz. The patients were asked to breath normally. B-mode and colour-Doppler ultrasound was first used to identify the target node, and a long axis view without a major artery nearby which otherwise can cause significant pulsatile motion. Then 1.2ml SonoVue (Bracco, Milan, Italy) microbubbles were administered intravenously as a 2 second bolus followed by a flush of saline. Clinical CEUS data were acquired for at least 80s after the injection, using a frame rate of 20Hz in CEUS mode and a mechanical index (MI) of 0.085. The bubble concentration was adjusted by a flash sequence on the system at an MI of 0.553 at 40s after injection, and a second flash was given if bubble concentration was judged high and individual bubbles could not be distinguished by visual assessment at 60s after injection. After the CEUS acquisition, ultrasound guided core needle biopsy was conducted according to the routine clinical management protocol. The pathological results received from biopsy were generated for comparison. 10 out of 44 patients' data sets were included for producing SRUS images through post-processing of the CEUS images as they met the following conditions (1) there is no large or significant out of plane motion; (2) the corresponding pathological diagnosis results were available; (3) length of useable video data with appropriate bubble concentration was >= 30s.

2.2 Post-processing for SRUS image

SRUS images were obtained through off-line post-processing of the acquired video sequences.

After motion correction [23], an intensity threshold was estimated by maximum entropy to remove the noise. To detect microbubbles in the images, only regions with features including shape, intensity and size that were inside the predefined ranges were accepted as single microbubble signal. The ranges of these features were determined by the variations of individual bubble signals measured in a lab phantom using a similar ultrasound setting. These detected microbubbles were localised and tracked over frames and accumulated to generate SRUS images. Each centroid position of detected microbubble was represented by a Gaussian profile in the localisation density map with a standard deviation of 10 μm, given by the localisation precision.

The tracking algorithm found the best correlated bubble signals within a search window between neighbouring frames [13]. For each bubble signal identified in frame n, the intensity cross correlation was calculated between that bubble and each of those bubbles found in frame n+1 within a search window. The bubbles in different frames with the maximum normalised cross correlation above an empirically determined threshold of 0.65 were paired. The search window size was defined according to the imaging frame rate and the maximum flow velocity of interest. Given the limited frame rate of 20Hz for the clinical system, and as we were mainly interested in the micro-vessels where typically the flow velocity is several millimetres per second, 600 micrometres was set as the maximum search range so that flow velocities of up to 12 mm/s could be tracked.

The detected bubbles and tracks were accumulated to generate the SRUS images and flow velocity and direction maps. The SRUS processing pipeline is described in supplementary Fig S1.

2.3 Quantifications from super-resolution ultrasound image

Vessel density

Vessel density is defined as the ratio of the total microvascular area in the binary LN SRUS microvascular map, and the total area of the region of interest (ROI). The ROI is a manually selected full 2D cross-section of the LN. The binary SRUS microvascular map was generated by detecting the pixels in the SRUS map with intensity higher than a localisation threshold of 0.5.

Vessel spatial complexity

Fractal dimension is a ratio providing a statistical index of complexity for a given structure/pattern. It is hypothesised that the microvascular structure associated with cancer would be more complex than that of normal tissue, and hence has higher fractal dimension. The fractal dimension of LN microvascular was used to quantify the complexity of the microvascular geometry and estimated by applying the frequently used box-counting method developed by Russel et al. [25].

Flow velocity and direction

Since microbubbles remain within the vascular space and have similar flow dynamics as red blood cells [26], the tracking of individual microbubbles was made to generate super-resolved maps of blood flow velocity and direction of the microvasculature.

Local Flow Direction Irregularity (LFDI)

The blood flow in malignant tumour is more likely to be disorganised. Therefore, a measure of how irregular local micro-flow is could be a promising marker for malignancy. This was only

made possible by the high resolution images of microvascular flow dynamics afforded by SRUS. We define Local Flow Direction Irregularity (LFDI) as the variance of flow direction within a defined local region/window:

$$Var(angle) = E[(angle - E(angle))^2]$$

Where E denotes the mathematical expectation, and angle denotes the flow direction obtained through super-resolved velocity mapping. The LFDI was calculated block-by-block for each non-overlapping 2 mm×2 mm block regions within the segmented LN ROI. The size of 2 mm block was defined according to the difference between micro-metastases (less than or equal to 2 mm) and macro-metastases (greater than 2 mm).

The mean and standard deviations of the different measures were generated from 4 reactive and 6 metastatic LN acquisitions. Student's two sample t-test was used to test the statistical significance of differences in the different image markers between metastatic and reactive LNs.

3. Results

Fig 1 shows B-mode, CEUS maximum intensity projection (MIP), and SRUS images of two example LNs. The LN ROI was indicated with the green line.

Supplementary Fig S2 illustrates that SRUS images contains more detailed morphological information which is not visible in the MIP image. Fig S2B and C show higher magnification of the same ROI from MIP and SRUS velocity map. The same ROI is indicated with the white box in Fig S2A.

Supplementary Fig S3 shows a comparison of a classical Doppler vascular image and the SRUS image of the same reactive LN. As can be seen in the Colour Doppler image, only major vessels

with fast blood flow (up to 6.7 cm/s) are visualised. In the corresponding SRUS velocity map, blood flow with much slower velocity can be detected.

Fig 2A and 2C shows the SRUS direction maps for the same two LNs as Fig 1. The corresponding LFDI maps are also visualised in Fig 2B and 2D. As can be seen from the figure, the reactive LN shown in Fig 2B has a lower LFDI and appears more homogeneous than that of the metastatic LN shown in Fig 2D.

Fig 3 displays measurements of micro-vessel density, fractal dimension, mean velocity and LFDI for the reactive and metastatic LNs. As can be seen, reactive LNs have a significant lower LFDI (1000 ± 376) than that of metastatic LNs (1600 ± 388, P = 0.0465). While the estimated micro-vessel density has a lower average value (31 ± 10%) in reactive LNs than that in metastatic LNs (42 ± 5%), no statistically significant difference was found. For the results of fractal dimension, reactive LNs have a similar value (1.75 ± 0.04) as that of the metastatic LNs (1.79 ± 0.05). The measured blood flow velocity has a slightly higher average (2.0 ± 0.7) for reactive LNs than that of metastatic LNs (1.8 ± 0.5), although the difference is again not statistically significant.

4. Discussion

Abnormal hemodynamics in tumour-associated vasculature can be a valuable imaging marker clinically, but currently there is a lack of an effective tool to evaluate this in vivo in deep tissue. As SRUS is able to generate microvascular morphology and flow velocity map with resolution at microscopic level, it allows the analysis of local hemodynamics in greater detail.

In this study we have, for the first time as far as we are aware, applied SRUS to evaluation of LNs in patients with lymphadenopathy using a clinical scanner. An image marker derived from the SRUS flow maps, Local Flow Direction Irregularity or LFDI, shows a statistically

significant difference between reactive and the metastatic LNs, even at a very low sample number (10 patients in total). This is encouraging, and consistent with our expectation of increased heterogeneity in hemodynamics in tumour-associated vasculature [27]. It should be noted that in Opacic [21] an entropy measure was used to characterise the local microvascular flow direction, similar to the LFDI measure presented in this work.

A number of other quantitative image markers derived from the SRUS images were also generated including micro-vessel density, micro-flow velocity, and vessel fractal dimension. As shown in Fig.3, the estimated micro-vessel density has a lower average value in reactive LNs than in metastatic LNs. This is consistent with the positive correlation between micro-vessel density and tumour occurrence which have been reported in previous studies [28]. However the difference is not statistically significant, likely due to the small number of samples and the different types of malignancies and locations of LNs used in this study. The data here contains five different types of malignancies from various body locations. Furthermore, the different time points since onset of the cancer for each patient is also a confounding factor. This has increased the variability of the data within each group. Previous studies using spectral Doppler sonography has shown increased flow velocity in reactive LNs [29]. Furthermore, it was reported that the overall blood flow velocity tends to be lower in tumours than in normal tissues [30]. These are consistent with the data shown here.

SRUS imaging offers visualisation and quantification of individual micro-vessels, not achievable in conventional modalities. These novel measures open new avenues for characterising metastatic LNs in order to inform patient management. The gold-standard procedure for LN staging is still surgical excision and histopathological assessment, despite the fact that many patients with cancer do not have LN metastases at the time of surgery, and that the procedure can result in complications. Our results demonstrate that SRUS as a non-

invasive imaging modality has potential to assist LN diagnosis. 2D imaging with a single slice of a LN which is a 3D structure certainly poses a risk of missing a micrometastasis. Multiple 2D slice acquisitions would reduce such risk, but this will reduce the time spent on each acquisition given the limited persistence of the bubble signals in vivo, and as a result the number of localisations and signal to noise ratio for each individual 2D SRUS image may be reduced. However, given that SRUS imaging requires low bubble concentration, it is possible to change from bolus to an infusion so sufficient amount of data from multiple planes can be acquired. Further clinical studies should be done to optimise the data acquisition for multiple 2D slices.

One limitation of this study is the low number of patients. In this study out of the 44 patient datasets, 34 were not used for SRUS processing, mainly due to out of plane or large motion (14 datasets), and also the usable video length with appropriate bubble concentration being less than 30s (20 datasets). The data acquisition protocol should be further optimised. A slightly longer acquisition time or acquisition at a later time after injection could generate data with more appropriate bubble concentration for SRUS. More training for the operators, as well as future full 3D imaging technologies, would help address the out of plane motion issue. Further development of more advanced post-processing would also help to make use of data with higher bubble concentrations and larger motions.

Another limitation of the study is that the super-resolved flow velocity tracking is limited to flow velocity of ~12mm/s or less. This is primarily due to the limited imaging frame rate available to the clinical system used. A higher frame rate system will allow flows in a broader range to be tracked. Additionally, while the flow velocities were calculated based on bubble pairs in this study, velocity estimation using Kalman filter based on multiple frames [21] may provide a more robust estimation. A further limitation of this study is that while we have

clinical diagnosis of the LNs in this study through core needle biopsy and pathology as part of the patients' clinical management, we do not have sufficient information to be able to generate a spatial correspondence between the pathology and the SRUS images.

5. Conclusion

In this study we have, for the first time as far as we are aware, applied SRUS to evaluation of LNs in patients with lymphadenopathy. Local microvascular flow direction irregularity has shown to be a promising marker for distinguishing metastatic LNs.

References

[1] L.-J. Liao, W.-C. Lo, W.-L. Hsu, C.-T. Wang, and M.-S. Lai, 'Detection of cervical lymph node metastasis in head and neck cancer patients with clinically N0 neck-a meta-analysis comparing different imaging modalities', BMC Cancer, v12, p236, 2012

[2] D. N. Krag et al., 'Sentinel-lymph-node resection compared with conventional axillary-lymph-node dissection in clinically node-negative patients with breast cancer: overall survival findings from the NSABP B-32 randomised phase 3 trial', Lancet Oncol., v11(10), p927–933 2010

[3] Li N, Cui M, Yu P, Li Q. Correlations of lncRNAs with cervical lymph node metastasis and prognosis of papillary thyroid carcinoma. Onco Targets Ther. 2019;12:1269-1278

[4] R. E. Mansel et al., 'Randomized Multicenter Trial of Sentinel Node Biopsy Versus Standard Axillary Treatment in Operable Breast Cancer: The ALMANAC Trial', JNCI J. Natl. Cancer Inst., v98(9), p599–609, 2006

[5] Carmeliet, P., Jain, R. Angiogenesis in cancer and other diseases. Nature 407, 249–257 (2000).

[6] Farnsworth, R., Lackmann, M., Achen, M. et al. Vascular remodeling in cancer. Oncogene 33, 3496–3505 (2014).

[7] Lindner, J. R. (2004). "Microbubbles in medical imaging: current applications and future directions." Nature Reviews Drug Discovery 3(6): 527-532.

[8] Sever, A., Jones, S., Cox, K., Weeks, J., Mills, P. and Jones, P. (2009), Preoperative localization of sentinel lymph nodes using intradermal microbubbles and contrast‐enhanced ultrasonography in patients with breast cancer. Br J Surg, 96: 1295-1299.

[9] L. Chen, L. Chen, J. Liu, B. Wang, and H. Zhang, 'Value of Qualitative and Quantitative Contrast-Enhanced Ultrasound Analysis in Preoperative Diagnosis of Cervical Lymph Node Metastasis From Papillary Thyroid Carcinoma', J. Ultrasound Med. Off. J. Am. Inst. Ultrasound Med., Jun. 2019

[10] M.-X. Tang et al., 'Quantitative contrast-enhanced ultrasound imaging: a review of sources of variability', Interface Focus, v1(4), p520–539, 2011

[11] C. Dudau et al., 'Can Contrast-Enhanced Ultrasound Distinguish Malignant from Reactive Lymph Nodes in Patients with Head and Neck Cancers?', Ultrasound Med. Biol., v40(4), p747–754, 2014

[12] Betzig E, Patterson GH, Sougrat R, Lindwasser OW, Olenych S, Bonifacino JS, Davidson MW, Lippincott-Schwartz J, Hess HF. Imaging intracellular fluorescent proteins at nanometer resolution. Science 2006;313:1642–1645.

[13] K Christensen-Jeffries, O Couture, PA. Dayton, YC. Eldar, K. Hynynen, F Kiessling, M. O'Reilly, GF. Pinton, G Schmitz, M-X Tang, M. Tanter and RJ.G.van Sloun, Super-resolution Ultrasound Imaging, Ultrasound in Medicine & Biology, V46(4) 2020, P865-891

[14] Siepmann M, Schmitz G, Bzyl J, Palmowski M, Kiessling F. Imaging tumor vascularity by tracing single microbubbles. 2011 IEEE IUS, 2011. p1906–1909.

[15] Christensen-Jeffries K, Browning RJ, Tang M-X, Dunsby C, Eckersley RJ. In vivo acoustic super-resolution and super-resolved velocity mapping using microbubbles. IEEE TMI 2015;34:433–440.

[16] Errico C, Pierre J, Pezet S, Desailly Y, Lenkei Z, Couture O, Tanter M. Ultrafast ultrasound localization microscopy for deep super-resolution vascular imaging. Nature 2015;527:499.

[17] Lin F, Shelton SE, Espíndola D, Rojas JD, Pinton G, Dayton PA. 3-D ultrasound localization microscopy for identifying microvascular morphology features of tumor angiogenesis at a resolution beyond the diffraction limit of conventional ultrasound. Theranostics 2017a;7:196.

[18] Song P, Trzasko JD, Manduca A, Huang R, Kadirvel R, Kallmes DF, Chen S. Improved super-resolution ultrasound microvessel imaging with spatiotemporal nonlocal means filtering and bipartite graph-based microbubble tracking. IEEE T UFFC 2017;65:149–167.

[19] Zhu J, Rowland EM, Harput S, Riemer K, Leow CH, Clark B, Cox K, Lim A, Christensen-Jeffries K, Zhang G. 3D Super-Resolution US Imaging of Rabbit Lymph Node Vasculature in Vivo by Using Microbubbles. Radiology 2019;291:642–650.

[20] Kanoulas, E; Butler, M; Rowley, C et al., Super-Resolution Contrast-Enhanced Ultrasound Methodology for the Identification of In Vivo Vascular Dynamics in 2D, Investigative Radiology: 2019 - V54(8), p500-516

[21] Opacic T, Dencks S, Theek B, Piepenbrock M, Ackermann D, Rix A, Lammers T, Stickeler E, Delorme S, Schmitz G. Motion model ultrasound localization microscopy for preclinical and clinical multiparametric tumor characterization. Nature communications 2018;9:1527.

[22] Zhang W, Lowerison MR, Dong Z, Miller RJ, Keller KA, Song P. Super-Resolution Ultrasound Localization Microscopy on a Rabbit Liver VX2 Tumor Model: An Initial Feasibility Study. Ultrasound Med Biol. 2021 Aug;47(8):2416-2429.

[23] Harput S, Christensen-Jeffries K, Brown J, Li Y, Williams KJ, Davies AH, Eckersley RJ, Dunsby C, Tang M-X. Two-Stage Motion Correction for Super-Resolution Ultrasound Imaging in Human Lower Limb. IEEE T UFFC 2018;65:803–814.

[24] Zhang, G., S. Harput, H. Hu, K. Christensen-Jeffries, J. Zhu, J. Brown, C. H. Leow, R. J. Eckersley, C. Dunsby, et M. Tang. « Fast Acoustic Wave Sparsely Activated Localization Microscopy: Ultrasound Super-Resolution Using Plane-Wave Activation of Nanodroplets ». IEEE T UFFC 66, no 6 (2019): 1039 46.

[25] D. A. Russell, J. D. Hanson, and E. Ott, 'Dimension of Strange Attractors', Phys. Rev. Lett., v45(14), p1175–1178, 1980

[26] Ismail Suad, Jayaweera Ananda R., Camarano Gustavo, Gimple Lawrence W., Powers Eric R., and Kaul Sanjiv, 'Relation Between Air-Filled Albumin Microbubble and Red Blood Cell Rheology in the Human Myocardium', Circulation, v94(3), p445–451, 1996,

[27] M. Leunig et al., ‘Angiogenesis, Microvascular Architecture, Microhemodynamics, and Interstitial Fluid Pressure during Early Growth of Human Adenocarcinoma LS174T in SCID Mice’, Cancer Res., v52(23), p6553–6560, 1992

[28] Saad, R., Kordunsky, L., Liu, Y. et al. Lymphatic microvessel density as prognostic marker in colorectal cancer. Mod Pathol 19, 1317–1323 (2006).

[29] A. T. Ahuja and M. Ying, ‘Sonographic Evaluation of Cervical Lymph Nodes’, Am. J. Roentgenol., v184(5), p1691–1699, 2005

[30] J. A. Nagy, S.-H. Chang, A. M. Dvorak, and H. F. Dvorak, ‘Why are tumour blood vessels abnormal and why is it important to know?’, Br. J. Cancer, v100(6), p865–869, 2009

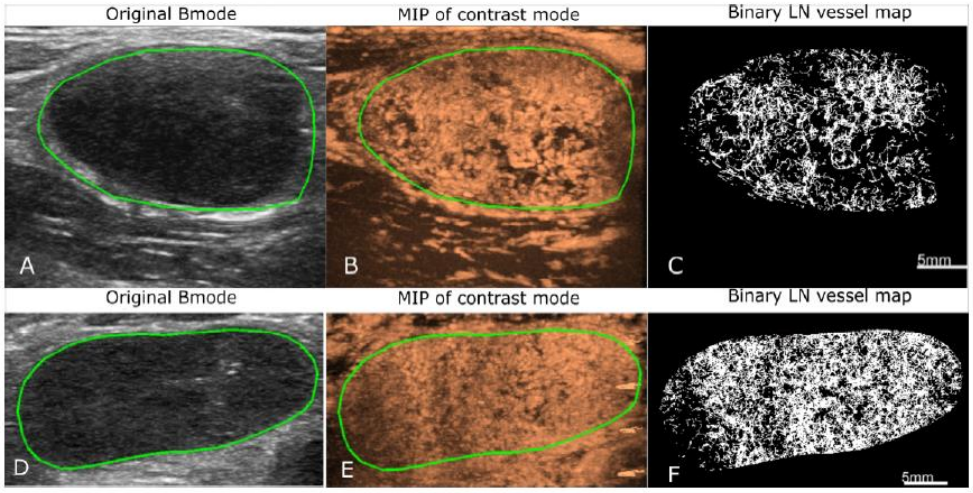

Figure 1: Images of two example LNs (A,B,C are from a reactive lymph node; D,E,F from a metastatic lymph node). A,D Conventional Bmode ultrasound, LN region of interest (ROI) is manually segmented from the original B-mode image as indicated by the green contour. B,E Maximum Intensity Projection (MIP) images of the LNs. C,F Super-resolution binary LN vessel map.

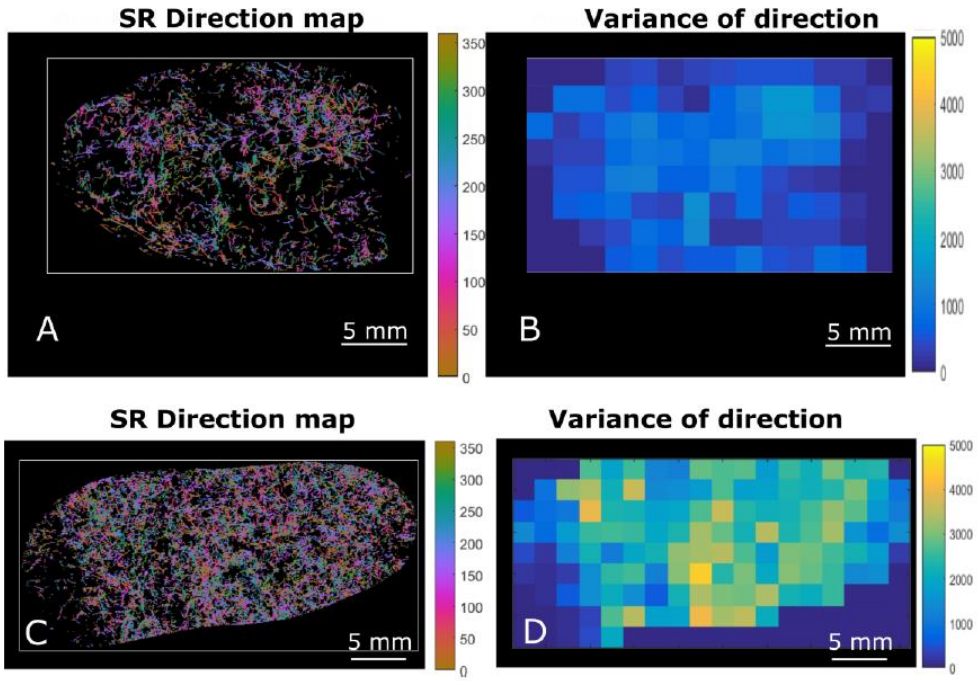

Figure 2: A,.C Super resolution flow direction maps of two LNs, where colour codes the angle of blood flow direction; B,D. Local Flow Direction Irregularity (LFDI) maps who a higher degree of irregularity in the metastatic LN in D comparing to the reactive LN in B.

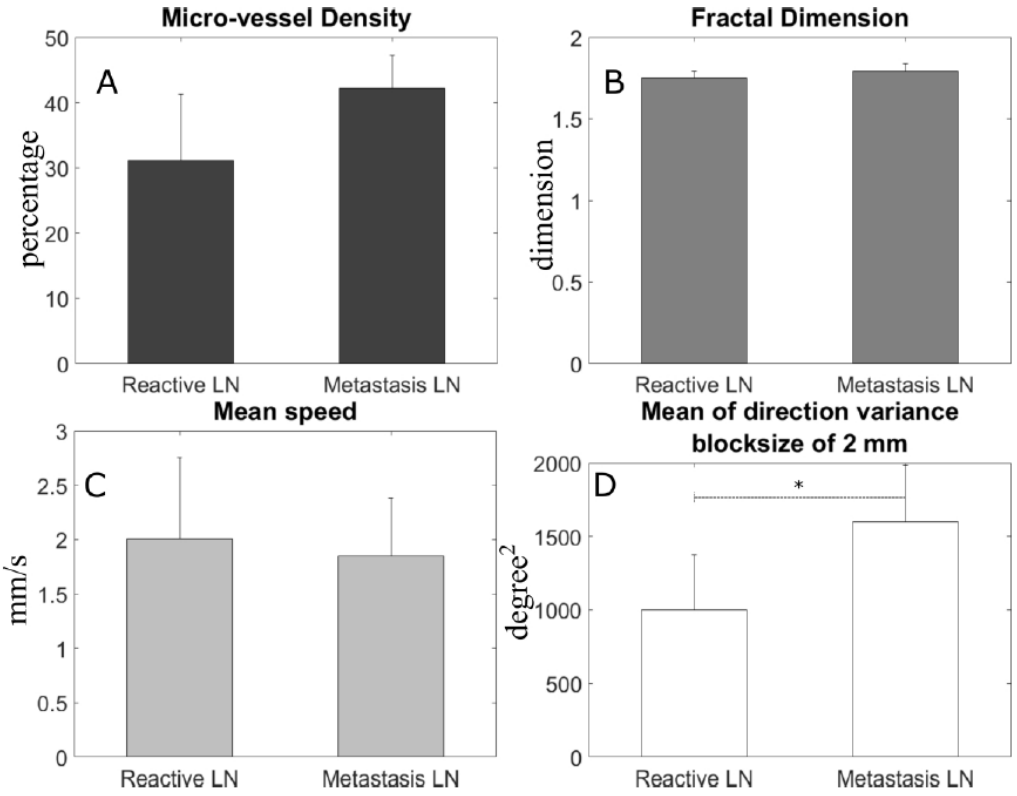

Figure 3: Quantification results in reactive (n=4) and metastasis (n=6) LNs: A, micro-vessel density. B, fractal dimension. C, mean speed and D, Local Flow Direction Irregularity (LFDI). Significant difference between reactive and metastatic LNs was only found in the LFDI ($P < 0.05$.).

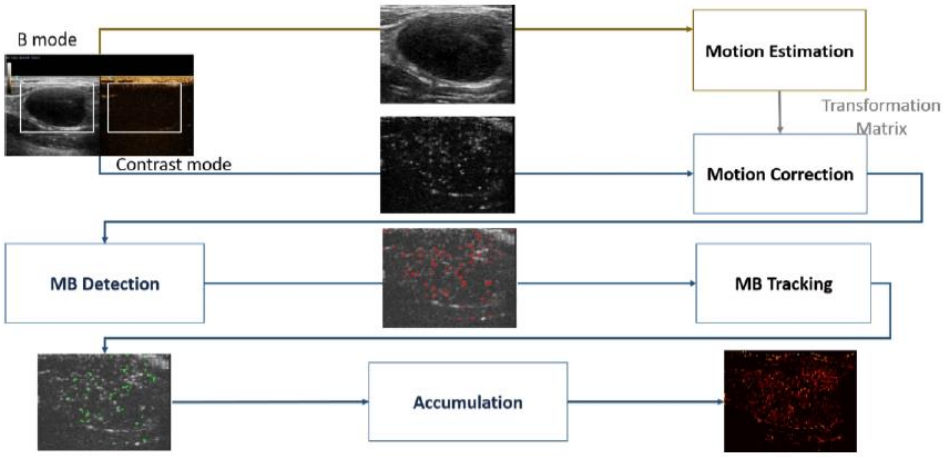

Figure S1: Post-processing pipeline for the production of SR ultrasound images. Motion estimation is performed on the B-mode ultrasound images, the generated transformation matrix is applied on the simultaneously acquired contrast-mode images to accomplish motion correction. After the motion correction, microbubbles are detected and tracked over frames. The final SR ultrasound images are obtained after accumulation.

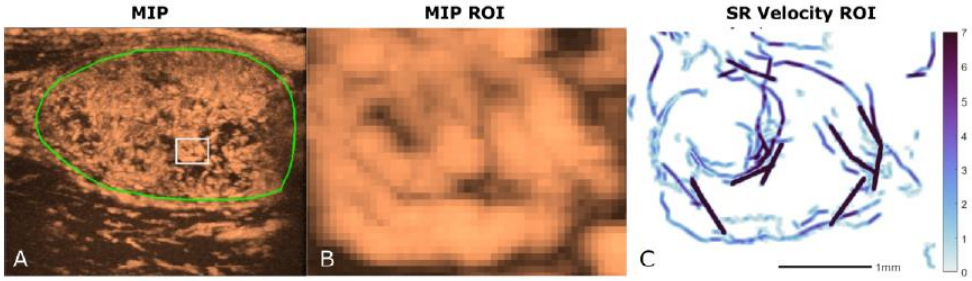

Figure S2: Comparison between maximum intensity projection (MIP) of contrast mode images and super resolution velocity map. A, MIP of the whole image, a small region of interest (ROI) is selected as indicated by the white box. B and C are the higher magnification of the same ROI from MIP and super resolution (SR) velocity map.

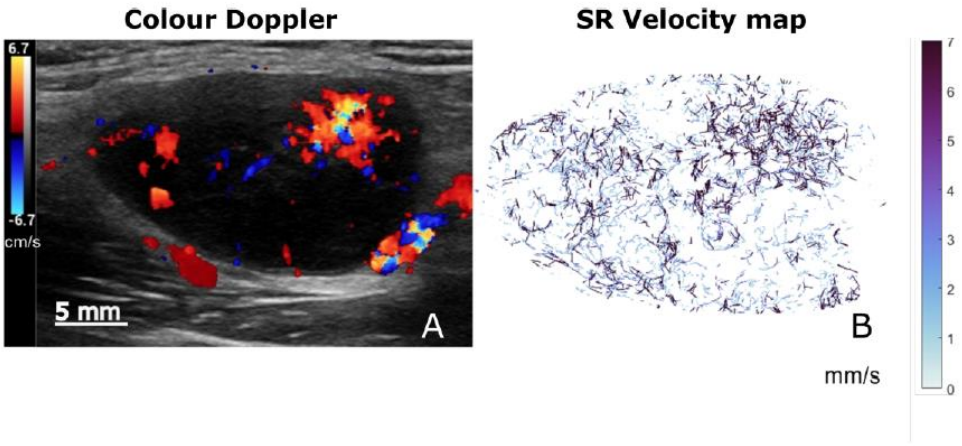

Figure S3: Comparison of the blood flow detected by colour Doppler (left) and super resolution velocity map (right).